Available online at www.sciencedirect.com
ScienceDirect
Trans. Nonferrous Met. Soc. China 33(2023) 619−631
Transactions of Nonferrous Metals Society of China
www.tnmsc.cn

Leaching kinetics of de-lithium residue from spent ternary lithium-ion battery cathodic materials with starch as reductant

Wei-lun LI[1], Yong-ming CHEN[1], Shuai LI[1], Chang-hong WANG[1], Yun LI[1], Tian-yu ZHAO[1,2], Michael TRAVERSY[2], Cong CHANG[1], Ya-fei JIE[1], Jing HE[1], Chao-bo TANG[1], Sheng-hai YANG[1]

1. School of Metallurgy and Environment, Central South University, Changsha 410083, China;
2. The Robert M. Buchan Department of Mining, Queen's University, 25 Union Street, Kingston, Ontario K7L3N6, Canada

Received 30 September 2021; accepted 8 July 2022

Abstract: Starch was employed as a reductant for the recovery of Ni, Co, and Mn from ternary lithium-ion batteries (LIBs) cathodic materials de-lithium residue, and the leaching kinetics and mechanism were studied. The effects of stirring speed, leaching temperature, H_2SO_4 concentration, and starch dosage on leaching efficiencies of Ni, Co, and Mn from de-lithium residue were systematically investigated. Optimized conditions (1.5 mol/L H_2SO_4, 6 g/L starch, stirring speed of 500 r/min, 80 °C and 60 min) yielded leaching efficiencies of 98.07%, 96.52%, and 98.06 %, for Ni, Co, and Mn, respectively. Apparent activation energies, described by the chemically controlled unreacted shrinking core model, were 93.32, 102.84, and 95.68 kJ/mol, for Ni, Co, and Mn, and their apparent reaction orders in H_2SO_4 were 0.9225, 1.0335, and 1.1285, respectively. Starch is abundant, affordable, and exceptionally alternative to conventional reductants for the recovery of valuable metals from spent ternary LIBs.

Key words: spent lithium-ion batteries; leaching kinetics; de-lithium residue; sulfuric acid–starch solution; chemical reaction control

1 Introduction

The rapid development of hybrid or full electric vehicles is accelerating the production, decommissioning, and recycling of lithium-ion batteries (LIBs) [1]. For example, ternary power LIBs contain large amounts of valuable metals, such as 5%−20% Co, 5%−12% Ni, 7%−10% Mn, and 2%−5% Li (mass fraction). This significant concentration of valuable metals qualifies spent ternary LIBs as a secondary resource, amenable to economic recovery through recycling [2]. Yet, toxic substances used in LIBs recycling are known to represent extreme environmental risk, and alternative approaches must be identified [3]. Innovation in spent LIB recycling promises to stabilize battery material supply chains and relieve the impacts of primary mining.

Recycling spent ternary LIBs is mainly based on two strategies: hydrometallurgy [4] and pyrometallurgy [5]. Compared with pyrometallurgy, hydrometallurgy is widely applied by many industries because of its low energy consumption and high recovery rate. The disposal process generally involves pretreatment [6], leaching [7], purification/separation [8], and preparation of product [9]. Leaching plays a critical role in the recycling process, and has attracted enormous attention because it influences the subsequent purification stage and the overall recovery of metals [1]. Spent LIBs are mainly leached to transfer the valuable metals from cathode active materials into the solution, using inorganic acids [10] (HCl, H_2SO_4, HNO_3, H_3PO_4, etc) and organic acids [11] (lactic acid, citric acid, tartaric

Corresponding author: Sheng-hai YANG, Tel: +86-13975894838, E-mail: yangshcsu@163.com
DOI: 10.1016/S1003-6326(22)66133-8

acid, DL-malic acid, oxalic acid, trichloroacetic acid (TCA), ascorbic acid, formic acid, acetic acid, etc). To improve the leaching efficiency, reductants (H_2O_2 [12], $NaHSO_3$ [13], and glucose [14]) are generally introduced to reduce high-valence metals (e.g., Co(III) and Mn(IV)).

Many studies on the leaching of spent ternary LIBs cathodes focus on the recovery of Li, Ni, Co, and Mn. However, these methods complicate subsequent steps, such as extraction and separation, which can also cause secondary pollution [15]. Previous leaching studies (Table 1) focused on determining the rate-controlling step and corresponding apparent activation energies, but failed to sufficiently describe process kinetics. H_2O_2 (a usual reductant) is expensive, unstable, and reacts violently in acidic solution [3]. Monosaccharides are an alternative reductant for the reductive leaching of spent LIBs [14]. Starch is a naturally biodegradable and non-toxic polysaccharide that can be directly extracted from plants, such as wheat and potatoes [25]. It is abundant, affordable, stable, and easily converted into monosaccharides by H_2SO_4 for using as a reductant [3]. Starch has been applied as a reductant in many green processes, such as the syntheses of flower-shaped silver nanoparticles (AgNPs) [26], uniform spherical AuNPs [27], and PtNPs [28]. Therefore, starch is a suitable reductant for leaching metals from de-lithium cathode powders.

In this study, starch was used as a reductant to decrease the influence of low-valence metals on leaching kinetics from de-lithium ternary LIBs cathode powder using H_2SO_4 lixiviant. The leaching efficiencies attained by starch were comparable to those achieved by H_2O_2, indicating that starch may be a suitable alternative reductant.

The effects of stirring speed (200−600 r/min), leaching temperature (50−90 °C), concentration of H_2SO_4 (0.25−2.0 mol/L), and starch dosage (1−10 g/L) on the leaching kinetics of the de-lithium residue were systematically investigated. The rate-controlling step, apparent activation energy, and reaction orders of the leaching reaction were determined. The mechanism of leaching kinetics in the H_2SO_4–starch solution was revealed through characterization of post-leaching solution (PLS) and residue.

2 Experimental

2.1 Materials and reagents

In this study, spent ternary LIBs powder was supplied by Hunan Reshine New Material Co., Ltd., China. Analytical grade starch and barium chloride ($BaCl_2$) were produced by Sinopharm Chemical Reagent Co., Ltd., China.

2.2 Leaching process

The leaching solutions were prepared from reagent-grade H_2SO_4 dissolved in deionized water to the desired H_2SO_4 concentration (0.25−2 mol/L). The leaching experiments were conducted in a 1000 mL three-necked round-bottom flask, fitted with a mercury thermometer, a delivery tube for the leaching solutions, and a reflux condenser to maintain solution volume.

Starch was added to dilute H_2SO_4 solution at a

Table 1 Summary of leaching kinetics of cathode material of ternary LIBs

Cathode material	Leaching reagent	Model and control step	Leaching efficiency/%				Reference
			Li	Ni	Co	Mn	
$LiNi_{1/3}Co_{1/3}Mn_{1/3}O_2$	DL-malic + H_2O_2	Chemical reaction and diffusion	98.9	94.3	95.1	96.4	[12]
	Acetic/maleic acid + H_2O_2	Diffusion controlled	98.39	97.27	97.72	97.07	[16]
			98.24	98.05	98.41	98.06	
	H_2SO_4 + H_2O_2	Chemical reaction	99.7	99.7	99.7	99.7	[17]
	Malic acid	Chemical reaction	100	99.87	99.58	99.82	[18]
	TCA + H_2O_2	Chemical reaction	99.7	93.0	91.8	89.8	[19]
	Formic acid + H_2O_2	Chemical reaction	98.22	99.96	99.96	99.95	[20]
	Lactic acid + H_2O_2	Chemical reaction	97.7	98.2	98.9	98.4	[21]
$LiNi_xCo_yMn_{1-x-y}O_2$	Acetic acid + H_2O_2	Diffusion and chemical reaction	99.97	92.67	93.62	96.32	[22]
	L-tartaric acid + H_2O_2	Chemical reaction	99.07	99.31	98.64	99.31	[23]
$LiNi_{0.5}Co_{0.2}Mn_{0.3}O_2$	H_2SO_4 + NH_4Cl	Chemical reaction	99.11	97.49	97.55	97.34	[24]

fixed temperature and stirred for 30 min. The de-lithium residue was added to the flask and the slurry was agitated with a magnetic stirrer. Next, 5 mL of the slurry was removed from the sampling port at selected intervals and filtered quickly. Subsequently, the filtrate (0.5 mL) was diluted to 250 mL for analyses. Then, the undissolved residue was washed with deionized water and vacuum dried. Since all the experiments were conducted at a liquid-to-solid ratio of 100 mL/g, the concentration of the leaching agent was considered unchanged during the leaching process.

The leaching efficiency of each valuable metal in the leachate was determined via Eq. (1):

$$\eta_{Me}=C_{Me}V/(mw_{Me})\times100\% \quad (1)$$

where η_{Me} is the metal element (Me) leaching efficiency for Ni, Co, and Mn in %; C_{Me} is metal concentration in mg/L; V is the volume of the leachate in L; m is the mass of de-lithium residue; and w_{Me} is the mass fraction of Me in the de-lithium residue in wt.%.

2.3 Analytical methods

The contents of each metal in the cathode powder (the de-lithium residue) and leaching solution were analyzed via inductively coupled plasma atomic emission spectroscopy (ICP-AES; ICPE−9800, Shimadzu Corporation, Japan). The phases of all samples were characterized by X-ray diffraction (XRD, Japan Rigaku Model TTRIII, 40 kV, 250 mA with Cu K_α radiation). The microscopic morphologies and the elemental distributions of all samples were analyzed via scanning electron microscopy (SEM) with energy-dispersive spectroscopy (EDS) by field-emission SEM (FESEM; MIRA 3 LMU, Tessken, USA). The profiles of all samples were analyzed by their backscattered electron micrographs (BEM) (Japan Jeol JSM−6360LV). The surface features of the elemental electron states of the de-lithium residue were determined by X-ray photoelectron spectroscopy (XPS, Thermo K-Alpha) with Al K_α X-ray radiation.

3 Results and discussion

3.1 Preparation of de-lithium residue

The cathode powder of the spent ternary LIBs was pretreated as follows. Firstly, the cathode powder was leached under the following conditions: temperature, 60 °C; H_2SO_4 concentration, 2 mol/L; stirring speed, 300 r/min; liquid-to-solid ratio, 5 mL/g; leaching time, 3 h. Soluble sulfate on the surface of the leaching residue was filtered and washed using 1 mol/L $BaCl_2$ solution until no sulfate could be detected. The filtered residue was washed, dehydrated by anhydrous ethanol, and kept in a vacuum oven for 12 h. Finally, the leaching residue was obtained after removal of lithium (the de-lithium residue).

The chemical compositions of the metal elements in the de-lithium residue were determined via ICP-AES, and the results are presented in Table 2. The Li content was only 0.76 wt.%, indicating extensive de-lithium.

Table 2 Main chemical compositions of de-lithium residue (wt.%)

Li	Ni	Co	Mn
0.76	19.50	16.30	30.10

The XRD pattern revealed that the de-lithium residue was composed of $Li(Ni_xCo_yMn_{1-x-y})O_2$, NiO_2, Co_3O_4, and $CO_xNi_{3-x}O_4$ (Fig. 1(a)). The SEM−EDS results (Fig. 1(b)) indicated that the de-lithium residue morphology included small, aggregated, irregularly shaped particles. Further, Ni, Co, Mn, and O were uniformly distributed on the surface of the oxide particles.

The XPS spectra of the de-lithium residue are shown in Figs. 2(a−d). Figure 2(b) shows that the Ni 2p spectrum exhibited four peaks; the two strong peaks at 854.89 and 872.54 eV corresponded to Ni $2p_{3/2}$ and $2p_{1/2}$, respectively. Combined with the two satellite peaks at 861.54 and 880.39 eV, it was assumed that Ni^{2+} and Ni^{3+} were present in the sample [29]. Figure 2(c) shows the Co 2p spectrum. The binding energies (BEs) of Co $2p_{1/2}$ and Co $2p_{3/2}$ were located at 795.44 and 780.39 eV, respectively. Furthermore, the difference between BEs of the spin-orbit splitting peaks of Co $2p_{1/2}$ and Co $2p_{3/2}$ was >15 eV, demonstrating the coexistence of Co^{2+} and Co^{3+} in the de-lithium residue [30]. Figure 2(d) shows the Mn 2p spectrum in which two major peaks with BEs of 642.24 and 653.99 eV were observed. This finding was correlated with the Mn^{4+} data, indicating its presence in the sample [31]. The valences of Ni, Co, and Mn in the de-lithium residue, as determined by XPS, were +2/+3, +2/+3, and +4, respectively (Fig. 2), indicating that these

metals existed in metal oxide covalent bond, which cannot be readily reduced.

3.2 Effects of operation parameters on leaching efficiencies

3.2.1 Effect of stirring speed

The effect of stirring speed on the leaching efficiencies of Ni, Co, and Mn was investigated. Figure 3 showed that the leaching efficiencies of Ni, Co, and Mn increased with the increasing stirring speed since the increase in the stirring speed could improve the external diffusion rate of ions. At a stirring speed of >500 r/min, the leaching efficiency of Mn demonstrated an increasing trend, although

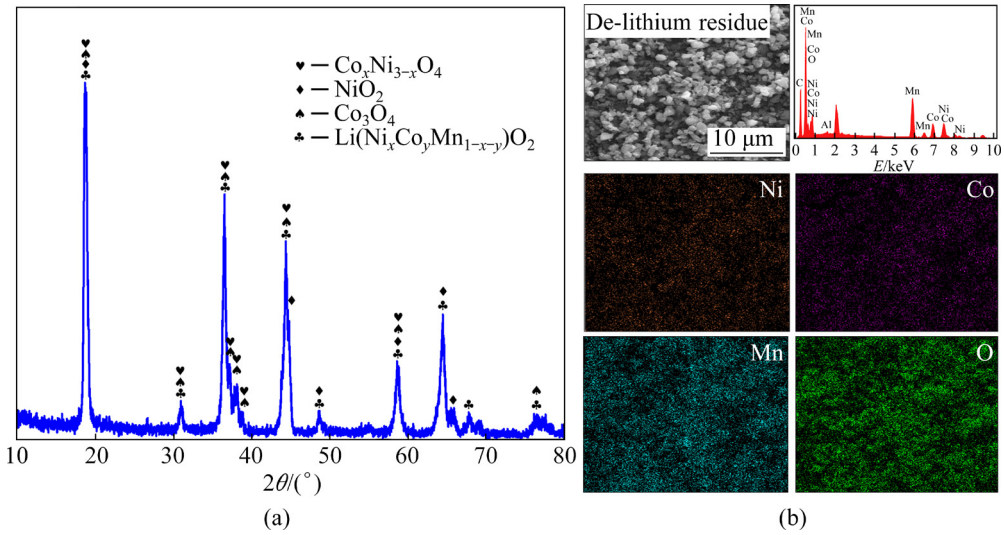

Fig. 1 XRD pattern (a) and SEM−EDS images (b) of de-lithium residues (raw materials for leaching experiments)

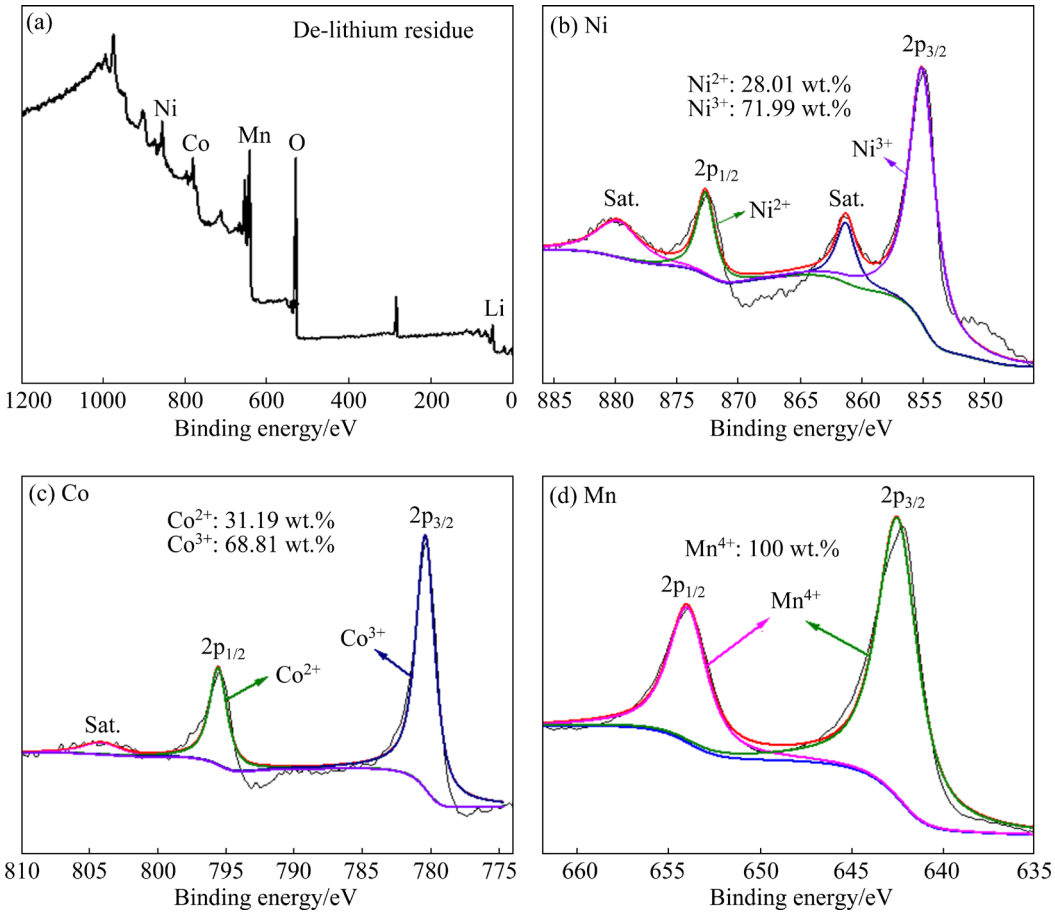

Fig. 2 XPS spectra of de-lithium residue sample: (a) Survey scan; (b−d) High-resolution spectra of Ni 2p, Co 2p, and Mn 2p, respectively

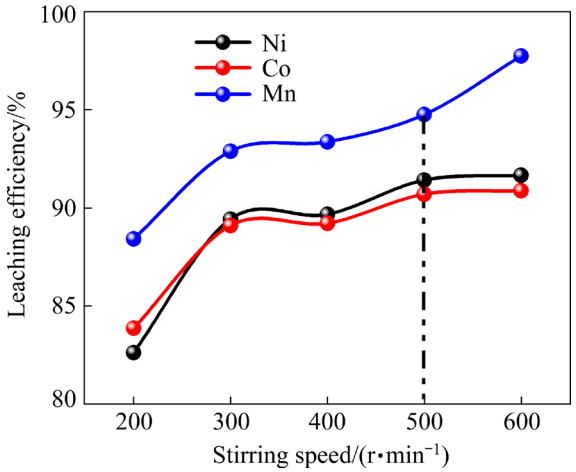

Fig. 3 Effect of stirring speed on leaching efficiencies (80 °C, 1.5 mol/L H_2SO_4, 10 g/L starch, and 20 min)

those of Ni and Co almost remained unchanged, indicating the elimination of the limiting effect of external diffusion. Based on the leaching efficiency and economy thinking, 500 r/min was adopted as the stirring speed in the subsequent experiments.

3.2.2 Effects of leaching time and temperature

The effects of leaching time and temperature on leaching efficiencies of Ni, Co, and Mn were also investigated. Figure 4 showed that the leaching efficiencies of the various metals increased with reaction time up to 20 min. However, under high-temperature conditions (>70 °C), the leaching efficiencies remained constant with the reaction time from 20 to 60 min, indicating the completion of the leaching process. The leaching efficiencies of Ni, Co, and Mn were improved with increasing leaching temperature from 50 to 90 °C. During leaching from 50 to 70 °C, the leaching efficiencies of Ni, Co, and Mn increased rapidly from 14.91%, 12.78%, and 11.71% to 89.93%, 88.88%, and 90.68%, respectively. Since increasing the leaching temperature promoted the reaction rate, it was concluded that the reaction was endothermic.

Notably, although the temperature significantly affected the leaching efficiency when it ≤70 °C, and when it was >70 °C the leaching efficiencies of Ni, Co, and Mn increased slowly. Moreover, a higher

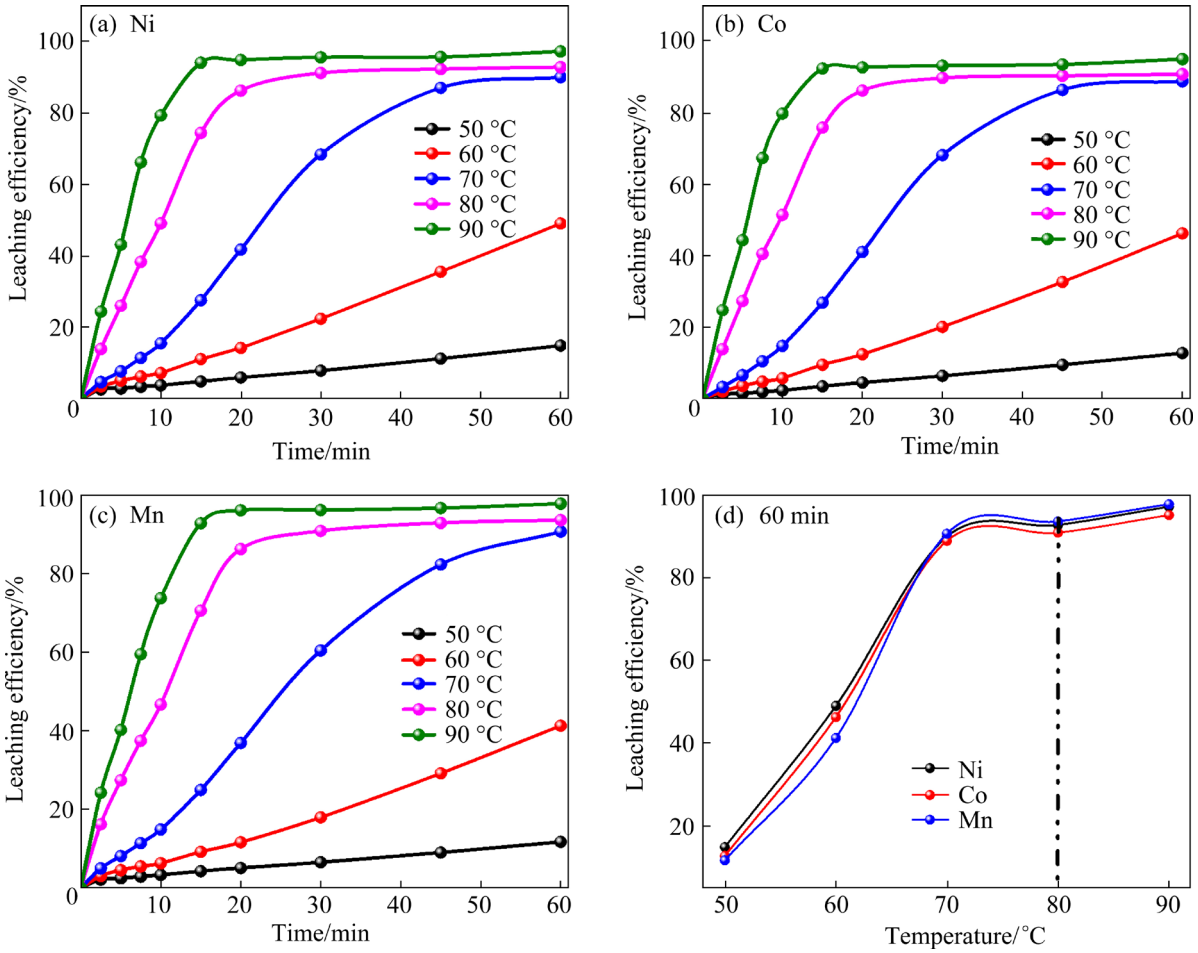

Fig. 4 Effects of leaching time and temperature on leaching efficiencies (500 r/min, 1.5 mol/L H_2SO_4, and 10 g/L starch)

reaction temperature resulted in an increased energy consumption. Thus, 80 °C was considered the optimum leaching temperature.

3.2.3 Effect of H_2SO_4 concentration

Figure 5 shows the effect of H_2SO_4 concentration on leaching efficiencies of Ni, Co, and Mn, which displayed a positive correlation at H_2SO_4 concentration <1.5 mol/L. The leaching efficiencies of Ni, Co, and Mn increased from 89.84%, 88.36%, and 86.19% to 96.41%, 95.76%, and 98.82%, respectively, when the concentration of H_2SO_4 increased from 0.25 to 1.5 mol/L. However, once the concentration of H_2SO_4 increased from 1.5 to 2.0 mol/L, the leaching efficiencies of Ni, Co, and Mn decreased to <93%. Perhaps, increasing the acid concentration increased the concentration gradient of H^+ on the particle surface, thereby promoting the leaching of Ni, Co, and Mn. However, a higher acid concentration might inhibit the diffusion of the leaching products, thereby affecting leaching [20,32]. Therefore, 1.5 mol/L was selected as the optimum concentration.

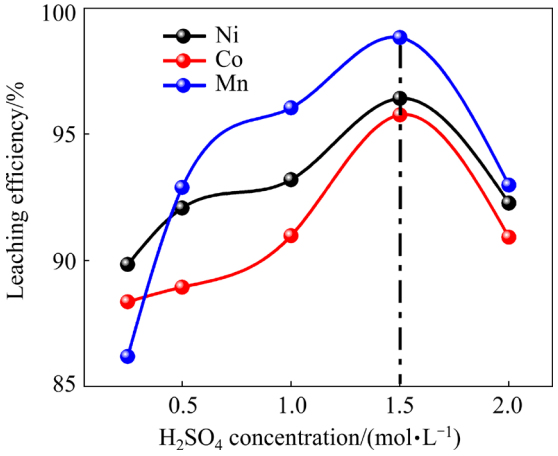

Fig. 5 Effect of H_2SO_4 concentration on leaching efficiencies (500 r/min, 80 °C, 10 g/L starch and 60 min)

3.2.4 Effect of starch dosage

Figure 6 showed that the leaching efficiencies of Ni, Co, and Mn increased with the increase of starch dosage. When the starch dosage changes from 1 to 6 g/L, the leaching efficiencies of Ni, Co, and Mn increased from 87.55%, 84.04%, and 64.04% to 95.88%, 94.01%, and 98.25%, respectively. This indicates that the increased starch dosage enhanced the reduction of high-valence Ni, Co, and Mn.

Given that the leaching reaction promoted the fracture of the Me—O covalent bond, Ni(III), Co(III), and Mn(IV) could be easily reduced to Me(II), easing their leaching [32,33]. However, when the starch dosage exceeded 6 g/L, the rapid leaching efficiency increment for Ni, Co, and Mn was depressed, indicating that 6 g/L was the optimum dosage of the reductant.

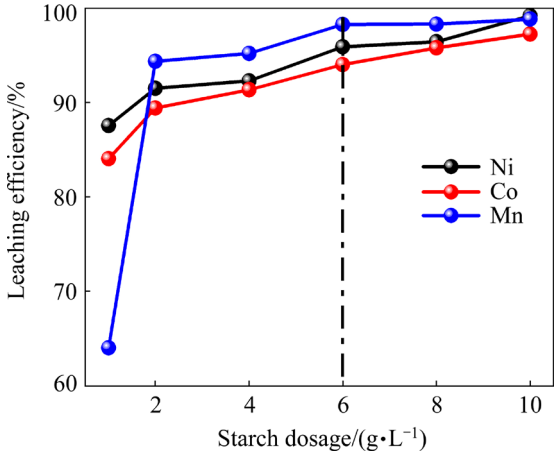

Fig. 6 Effect of starch dosage on leaching efficiencies (500 r/min, 80 °C, 1.5 mol/L H_2SO_4, and 60 min)

3.2.5 Validation experiments

Three large-scale leaching experiments were conducted under the optimum conditions based on the above results. Additionally, the solution volume was expanded to 3 L, and the reactant dosages were scaled up accordingly.

Figure 7 showed that the mean leaching efficiencies of Ni, Co, and Mn were 98.07%, 96.52%, and 98.06%, respectively. Compared with the results reported in Table 1, using starch as a

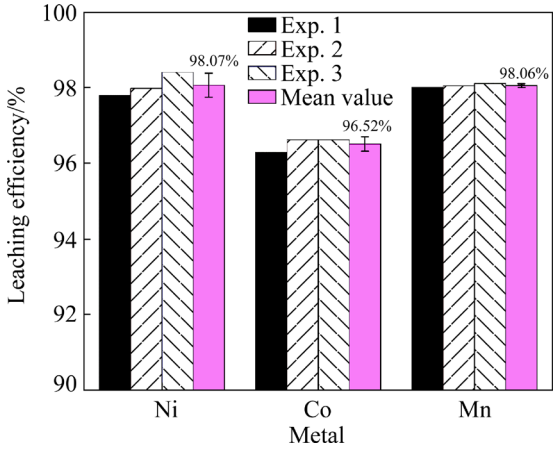

Fig. 7 Validation experiment results of leaching efficiencies of de-lithium residue (leaching conditions: stirring speed, 500 r/min; leaching temperature, 80 °C; H_2SO_4 concentration, 1.5 mol/L; starch dosage, 6 g/L; leaching time, 60 min)

reductant yielded similar leaching efficiencies to those achieved by H_2O_2. Further, the excellent reproducibility of the experiment was proved. This demonstrated that the leaching reaction could achieve high efficiency in a relatively short time if starch was employed as a reductant.

3.3 Reductive leaching kinetics of de-lithium residue in H_2SO_4–starch solution

3.3.1 Selection of leaching reaction mechanism and kinetic model

The XRD patterns of the de-lithium and leaching residues were obtained under the optimum conditions at different leaching time (Fig. 8). All samples exhibited a hexagonal α-$NaFeO_2$ structure with a space group of $R\bar{3}m$. Concurrently, the intensities of the major peaks of the residue containing high-valence Ni, Co, and Mn decreased with increasing leaching time.

The leaching residue samples, obtained under the optimum conditions at different leaching time (0−20 min), were characterized by SEM (Figs. 9(a−d)) and BEM (Figs. 9(e−h)). The de-lithium residue was the primary particle exhibiting an irregular shape and extremely small size (Fig. 9(a)). Figures 9(b−d) showed the SEM images of the leaching residue. After leaching in the H_2SO_4–starch solution, the de-lithium residue was wrapped by glucose (hydrolyzed by the starch), and a sugar-polymerized film was formed on the surface, facilitating the agglomeration of the primary particles into a spherical shape. A negative correlation was observed between the particle size

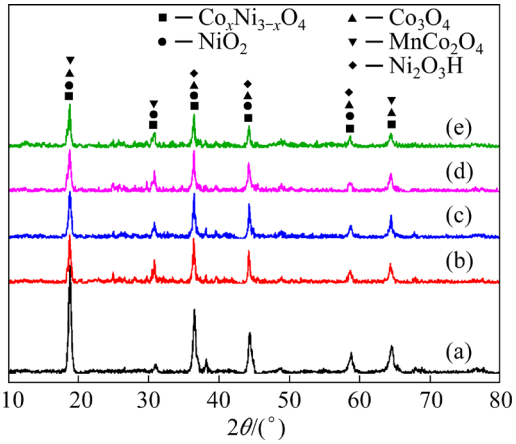

Fig. 8 XRD patterns of de-lithium residues before leaching (a), and leaching residues after reacting for 2.5 min (b), 10 min (c), 20 min (d), and 60 min (e) (the experimental conditions matching those in Section 3.2.5)

and reaction time, indicating that the lixiviant continuously reacted with the particles on the surface. The BEM images (Figs. 9(e−h)) of the polished de-lithium residue thin section before and after leaching indicated that the product layer did not appear at the edge of the leaching residue with decreasing particle size [34]. Combined with Figs. 9(b−d), it was deduced that the leaching process was consistent with the unreacted shrinking core model (USCM).

Based on the results of the above-described conditional leaching experiments, the leaching reaction was completed in about 15 min. Therefore, the leaching kinetics of the de-lithium residue was studied in H_2SO_4–starch solution for 15 min. The

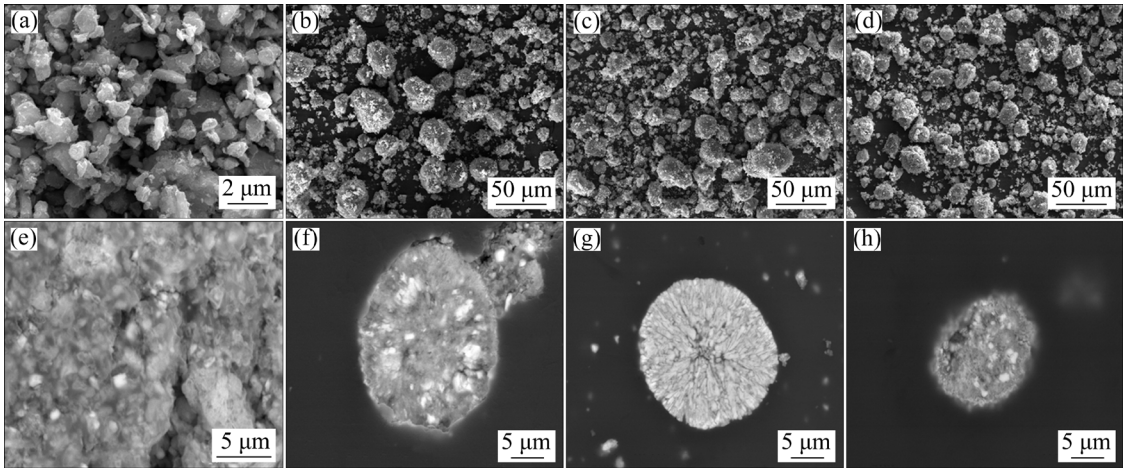

Fig. 9 SEM (a–d) and BEM (polished section) (e–h) images of de-lithium residues before leaching (a, e), and leaching residues after reacting for 2.5 min (b, f), 10 min (c, g), and 20 min (d, h) (experimental conditions matching those reported in Section 3.2.5)

principle of the leaching reaction is illustrated in Fig. 10. The generated CO_2 gas could be collected by electrochemical CO_2 capture technology [35].

The leaching reaction of the de-lithium residue corresponded to a liquid–solid heterogeneous mechanism, not involving a solid product layer; it proceeded at the liquid–solid phase interface. Many kinetic models have been applied to describing the metallurgical leaching process, and the most common model is USCM. A comparison of the SEM (Figs. 9(a–d)) and BEM (Figs. 9(e–h)) images of the de-lithium and leaching residues indicated that the particle size of the residue decreased with the increasing leaching efficiencies of Ni, Co, and Mn, demonstrating that the suitability of USCM in describing the leaching process.

3.3.2 Reductive leaching kinetics

The accuracy of this model was verified by plotting $1-2X/3-(1-X)^{2/3}$ and $1-(1-X)^{1/3}$ (X is the leaching efficiency) versus time t at different temperatures, H_2SO_4 concentrations, and starch dosages, and the results demonstrated that the model of the surface chemical reaction control ($1-(1-X)^{1/3}$ versus t) was superior to that of liquid-film diffusion control on the surfaces of the particles.

The results of $1-(1-X)^{1/3}$ versus time t at different temperatures, H_2SO_4 concentrations, and starch dosages are shown in Figs. 11(a, b, c), respectively.

Figures 11(a, b, c) showed that $1-(1-X)^{1/3}$ exhibited a good linear relationship with time t. Thus, the model of the surface chemical reaction control can be employed to describe the leaching kinetics of the de-lithium residue in the H_2SO_4–starch solution.

By fitting the linear regression of $1-(1-X)^{1/3}$ and time t in Fig. 11(a), the slopes of all the lines were obtained at different temperatures. According to the Arrhenius formula,

$$k=A\exp[-E_a/(RT)] \quad (2)$$

where k is the reaction rate constant at temperature T, A is the prefactor, T is the thermodynamic temperature, R is the molar gas constant, and E_a is the apparent reaction activation energy.

$\ln k$ was plotted against $1/T$, and the result is shown in Fig. 12(a). The determined E_a values of Ni, Co, and Mn during leaching were 93.32, 102.84, and 95.68 kJ/mol, respectively, based on the slope of the fitting line in Fig. 12(a). The leaching reaction was further confirmed to be a chemical reaction control based on its E_a.

The slope of the lines obtained by fitting the linear regression of $1-(1-X)^{1/3}$ and time t (Fig. 11(b)) is the value of k at different H_2SO_4 concentrations. $\ln k$ was plotted against $\ln C$ (H_2SO_4), and the results are shown in Fig. 12(b).

Figure 12(b) showed that the equations of the reaction rates of Ni, Co, and Mn were $\ln k=0.9225\ln C-3.7039$, $\ln k=1.0335\ln C-3.7164$, and $\ln k=1.1285\ln C-3.7790$, respectively; the slope values, 0.9225, 1.0335, and 1.1285, were the apparent reaction orders of the H_2SO_4 leaching reaction.

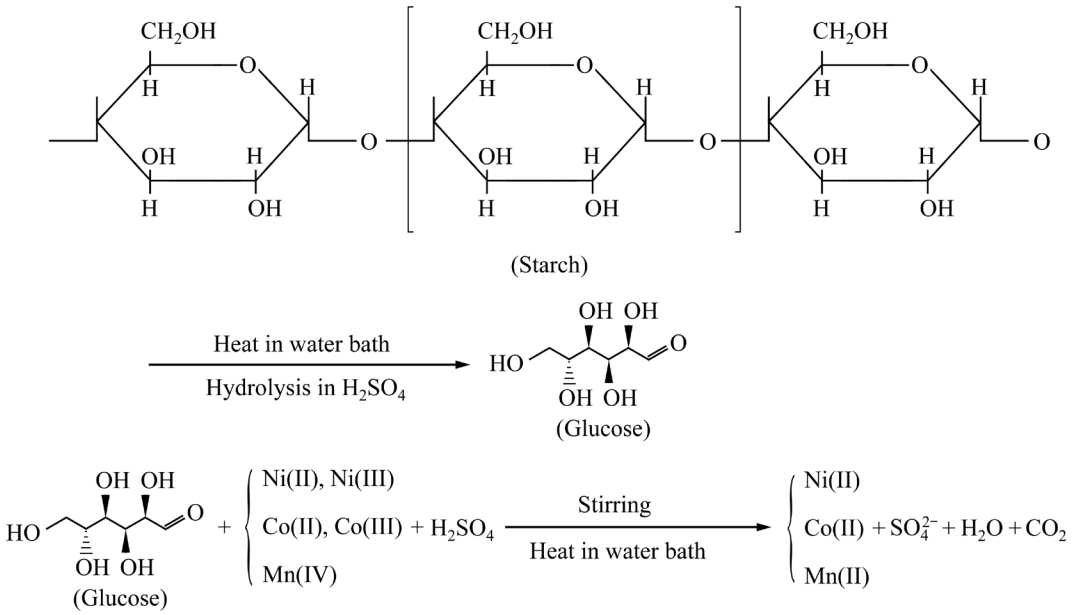

Fig. 10 Reaction principles of de-lithium residue in H_2SO_4−starch solutions

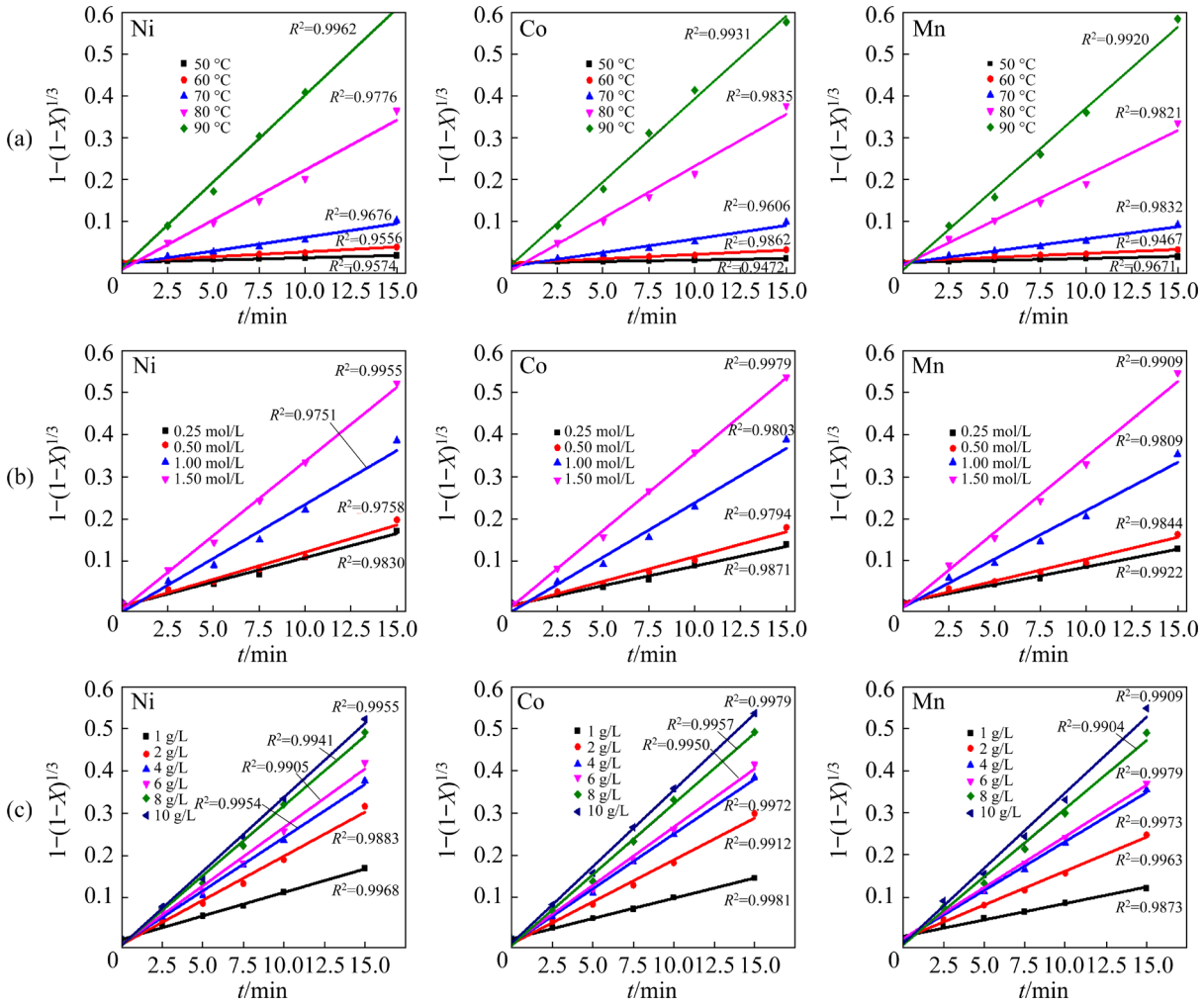

Fig. 11 Plots of $1-(1-X)^{1/3}$ versus t for de-lithium residues under different conditions in H_2SO_4–starch solution: (a) Temperature; (b) H_2SO_4 concentration; (c) Starch dosage

The apparent reaction speed constant, k, was a function of the H_2SO_4 concentration, starch dosage, stirring speed, and temperature, and can be expressed by combining Eq. (3) with the revised Arrhenius equation, as follows [36]:

$$K=k_0C_{H_2SO_4}^{a}C_{starch}^{b}W^{c}\exp[-E_a/(RT)] \quad (3)$$

where k_0 is the frequency factor, $C_{H_2SO_4}$ and C_{starch} are the concentrations of H_2SO_4 and starch dosage, respectively, W is the stirring speed, a is the H_2SO_4 concentration reaction order, b is the starch-dosage reaction order, and c is the influence index of the stirring speed. Since the stirring speed exerted only a slight effect on the de-lithium residue leaching efficiency in the H_2SO_4–starch solution, the influence index of the stirring speed was zero.

The experimental data under different conditions were substituted into Eq. (3). Figure 12(d) showed that a good linear relationship was established between the $1-(1-X)^{1/3}$ and $C_{H_2SO_4}^{a}C_{starch}^{b}W^{c}\exp[-E_a/(RT)]t$ of Ni, Co, and Mn in all the experimental data; the data points were mostly distributed around a line with relatively high parameters of R^2 for Ni (0.9853), Co (0.9907), and Mn (0.9885).

According to the above kinetic data fitting, the kinetic equations of Ni, Co, and Mn leaching in the H_2SO_4–starch solution of the de-lithium residue were obtained as follows, respectively:

$$1-(1-X)^{1/3}=4.8571\times10^{11}C_{H_2SO_4}^{0.9225}C_{starch}^{0.5075}\cdot\exp[-93319/(RT)]\cdot t \quad (4)$$

$$1-(1-X)^{1/3}=1.0074\times10^{13}C_{H_2SO_4}^{1.0335}C_{starch}^{0.5856}\cdot\exp[-102839/(RT)]\cdot t \quad (5)$$

$$1-(1-X)^{1/3}=6.7319\times10^{11}C_{H_2SO_4}^{1.1285}C_{starch}^{0.6662}\cdot\exp[-95681/(RT)]\cdot t \quad (6)$$

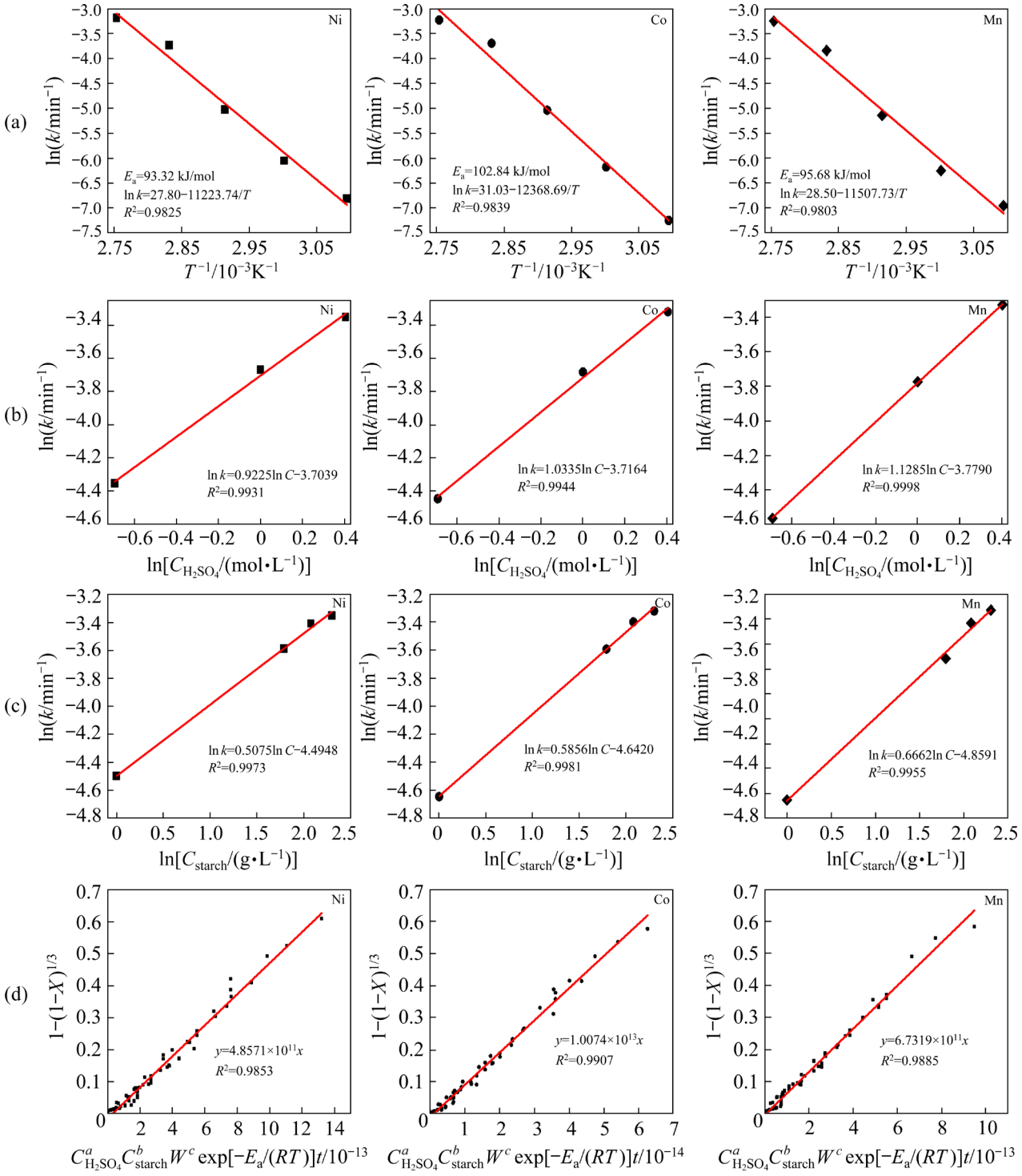

Fig. 12 Arrhenius plots of ln k versus T^{-1} (a), ln k versus ln $C_{H_2SO_4}$ (b), ln k versus ln C_{starch} (c) and relationship between 1−(1−X)$^{1/3}$ and $C^a_{H_2SO_4}C^b_{starch}W^c\exp[-E_a/(RT)]t$ (d)

4 Conclusions

(1) The leaching efficiencies of Ni, Co, and Mn were slightly enhanced by the increasing stirring speed, although they increased significantly with the increase of the temperature, H_2SO_4 concentration, and starch dosage. Under the optimized conditions, the leaching efficiencies of Ni, Co, and Mn were 98.07%, 96.52%, and 98.06%, respectively.

(2) The XRD results demonstrated that the

strong diffraction peaks of the leaching residue were gradually weakened as the leaching reaction progressed. The particle size of the de-lithium residue decreased continuously in the SEM and BEM images, being correlated with the USCM of the liquid–solid reaction in the metallurgical process.

(3) The leaching with the chemical reaction was demonstrated as the controlled step by USCM. The determined E_a values of the leaching reactions of Ni, Co, and Mn were 93.32, 102.84, and 95.68 kJ/mol, respectively, and the calculated apparent reaction orders of H_2SO_4 concentration were 0.9225, 1.0335, and 1.1285, respectively. Therefore, the kinetic equations of the Ni, Co, and Mn leaching reactions in the H_2SO_4–starch solution of the de-lithium residue were also obtained. Starch is an available, cost, and excellent alternative to traditional reductants for the recovery of valuable metals from spent LIBs.

Acknowledgments

This work was financially supported by the Anhui Province Innovative Engineering Project for New Energy Vehicles and Intelligent Connected Vehicles, China. The authors would like to acknowledge the funding support from the Research Fund Program of State Key Laboratory of Rare Metals Separation and Comprehensive Utilization, China (No. GK-201806). The authors also appreciate the editors and anonymous reviewers for their constructive comments and suggestions.

References

[1] LI L, ZHANG X X, LI M, CHEN R J, WU F, AMINE K, LU J. The recycling of spent lithium-ion batteries: A review of current processes and technologies [J]. Electrochemical Energy Reviews, 2018, 1: 461−482.

[2] ZOU Hai-yang, GRATZ E, APELIAN D, WANG Yan. A novel method to recycle mixed cathode materials for lithium ion batteries [J]. Green Chemistry, 2013, 15: 1183−1191.

[3] LAI Yan-qing, YANG Jian, ZHANG Gang, TANG Yi-wei, JIANG Liang-xing, YANG Sheng-hai, LI Jie. Optimization and kinetics of leaching valuable metals from cathode materials of spent ternary lithium ion batteries with starch as reductant [J]. The Chinese Journal of Nonferrous Metals, 2019, 29(1): 153−160. (in Chinese)

[4] MESHRAM P, PANDEY B D, MANKHAND T R. Extraction of lithium from primary and secondary sources by pre-treatment, leaching and separation: A comprehensive review [J]. Hydrometallurgy, 2014, 150: 192−208.

[5] REN Guo-xing, XIAO Song-wen, XIE Mei-qiu, PAN Bing, CHEN Jian, WANG Feng-gang, XIA Xing. Recovery of valuable metals from spent lithium ion batteries by smelting reduction process based on $FeO−SiO_2−Al_2O_3$ slag system [J]. Transactions of Nonferrous Metals Society of China, 2017, 27(2): 450−456.

[6] LI Wei-lun, YANG Sheng-hai, LIU Nan-nan, CHEN Yong-ming, XI Yan, LI Shuai, JIE Ya-fei, HU Fang. Study on vacuum pyrolysis process of cathode sheets from spent lithium-ion batteries [C]//Conference on Manufacturing the Circular Materials Economy, 2019. San Antonio, TX: TMS, 2019: 421−435.

[7] JHA M K, KUMARI A, JHA A K, KUMAR V, HAIT J, PANDEY B D. Recovery of lithium and cobalt from waste lithium ion batteries of mobile phone [J]. Waste Management, 2013, 33: 1890−1897.

[8] ZHU Shu-guang, HE Wen-zhi, LI Guang-ming, ZHOU Xu, ZHANG Xiao-jun, HUANG Ju-wen. Recovery of Co and Li from spent lithium-ion batteries by combination method of acid leaching and chemical precipitation [J]. Transactions of Nonferrous Metals Society of China, 2012, 22: 2274−2281.

[9] CHEN Ya, TIAN Qian-qiu, CHEN Bai-zhen, SHI Xi-chang, LIAO Ting. Preparation of lithium carbonate from spodumene by a sodium carbonate autoclave process [J]. Hydrometallurgy, 2011, 109: 43−46.

[10] LAROUCHE F, TEDJAR F, AMOUZEGAR K, HOULACHI G, BOUCHARD P, DEMOPOULOS G P, ZAGHIB K. Progress and status of hydrometallurgical and direct recycling of Li-ion batteries and beyond [J]. Materials, 2020, 13(3): 801−845.

[11] YANG Jian, JIANG Liang-xing, LIU Fang-yang, JIA Ming, LAI Yan-qing. Reductive acid leaching of valuable metals from spent lithium-ion batteries using hydrazine sulfate as reductant [J]. Transactions of Nonferrous Metals Society of China, 2020, 30(8): 2256−2264.

[12] SUN Cong-hao, XU Li-ping, CHEN Xiang-ping, QIU Tian-yun, ZHOU Tao. Sustainable recovery of valuable metals from spent lithium-ion batteries using DL-malic acid: Leaching and kinetics aspect [J]. Waste Management & Research, 2018, 36: 113−120.

[13] MESHRAM P, PANDEY B D, MANKHAND T R. Hydrometallurgical processing of spent lithium ion batteries (LIBs) in the presence of a reductant with emphasis on kinetics of leaching [J]. Chemical Engineering Journal, 2015, 281: 418−427.

[14] PAGNANELLI F, MOSCARDINI E, GRANATA G, CERBELLI S, AGOSTA L, FIERAMOSC A. Acid reducing leaching of cathodic powder from spent lithium ion batteries: Glucose oxidative pathways and particle area evolution [J]. Journal of Industrial and Engineering Chemistry, 2014, 20: 3201−3207.

[15] PENG Chao, HAMUYUNI J, WILSON B P, LUNDSTRÖM M. Selective reductive leaching of cobalt and lithium from industrially crushed waste Li-ion batteries in sulfuric acid

system [J]. Waste Management, 2018, 76: 582−590.

[16] LI Li, BIAN Yi-fan, ZHANG Xiao-xiao, XUE Qing, FAN Er-sha, WU Feng, CHEN Ren-jie. Economical recycling process for spent lithium-ion batteries and macro- and micro-scale mechanistic study [J]. Journal of Power Sources, 2018, 377: 70−79.

[17] HE Li-po, SUN Shu-ying, SONG Xing-fu, YU Jian-guo. Leaching process for recovering valuable metals from the $LiNi_{1/3}Co_{1/3}Mn_{1/3}O_2$ cathode of lithium-ion batteries [J]. Waste Management, 2017, 64: 171−181.

[18] MENG Qi, ZHANG Ying-jie, DONG Peng, LIANG Feng. A novel process for leaching of metals from $LiNi_{1/3}Co_{1/3}Mn_{1/3}O_2$ material of spent lithium ion batteries: Process optimization and kinetics aspects [J]. Journal of Industrial and Engineering Chemistry, 2018, 61: 133−141.

[19] ZHANG Xi-hua, CAO Hong-bin, XIE Yong-bing, NING Peng-ge, AN Hui-jiao, YOU Hai-xia, NAWAZ F. A closed-loop process for recycling $LiNi_{1/3}Co_{1/3}Mn_{1/3}O_2$ from the cathode scraps of lithium-ion batteries: Process optimization and kinetics analysis [J]. Separation and Purification Technology, 2015, 150: 186−195.

[20] GAO Wen-fang, ZHANG Xi-hua, ZHENG Xiao-hong, LIN Xiao, CAO Hong-bin, ZHANG Yi, SUN Zhi. Lithium carbonate recovery from cathode scrap of spent lithium-ion battery: A closed-loop process [J]. Environmental Science & Technology, 2017, 51: 1662−1669.

[21] LI Li, FAN Er-sha, GUAN Yi-biao, ZHANG Xiao-xiao, XUE Qing, WEI Lei, WU Feng, CHEN Ren-jie. Sustainable recovery of cathode materials from spent lithium-ion batteries using lactic acid leaching system [J]. ACS Sustainable Chemistry & Engineering, 2017, 5: 5224−5233.

[22] GAO Wen-fang, ZHANG Xi-hua, ZHENG Xiao-hong, LIN Xiao, CAO Hong-bin, ZHANG Yi, SUN Zhi. Selective recovery of valuable metals from spent lithium-ion batteries—Process development and kinetics evaluation [J]. Journal of Cleaner Production, 2018, 178: 833−845.

[23] HE Li-po, SUN Shu-ying, MU Yan-yu, SONG Xing-fu, YU Jian-guo. Recovery of lithium, nickel, cobalt, and manganese from spent lithium-ion batteries using l-tartaric acid as a leachant [J]. ACS Sustainable Chemistry & Engineering, 2017, 5: 714−721.

[24] LV Wei-guang, WANG Zhong-hang, CAO Hong-bin, ZHENG Xiao-hong, JIN Wei, ZHANG Yi, SUN Zhi. A sustainable process for metal recycling from spent lithium-ion batteries using ammonium chloride [J]. Waste Management, 2018, 79: 545−553.

[25] WANG Y J, TRUONG V D, WANG L F. Structures and rheological properties of corn starch as affected by acid hydrolysis [J]. Carbohydrate Polymers, 2003, 52: 327−333.

[26] PONSANTI K, TANGNORAWICH B, NGERNYUANG N, PECHYEN C. A flower shape-green synthesis and characterization of silver nanoparticles (AgNPs) with different starch as a reductant [J]. Journal of Materials Research and Technology, 2020, 9(5): 11003−11012.

[27] PIENPINIJTHAM P, THAMMACHAROEN C, EKGASIT S. Green synthesis of size controllable and uniform gold nanospheres using alkaline degradation intermediates of soluble starch as reductant and stabilizer [J]. Macromolecular Research, 2012, 20(12): 1281−1288.

[28] TONGSAKUL D, WONGRAVEE K, THAMMA-CHAROEN C, EKGASIT S. Enhancement of the reduction efficiency of soluble starch for platinum nanoparticles synthesis [J]. Carbohydrate Research, 2012, 357: 90−97.

[29] CHAI Zuo-qiang, WANG Zhi-xing, WANG Jie-xi, LI Xin-hai, GUO Hua-jun. Potentiostatic deposition of nickel cobalt sulfide nanosheet arrays as binder-free electrode for high-performance pseudocapacitor [J]. Ceramics International, 2018, 44: 15778−15784.

[30] SHEN Lai-fa, WANG Jie, XU Gui-yin, LI Hong-sen, DOU Hui, ZHANG Xiao-gang. $NiCo_2S_4$ nanosheets grown on nitrogen-doped carbon foams as an advanced electrode for supercapacitors [J]. Advanced Energy Materials, 2015, 5: 1400977.

[31] TREUIL N, LABRUGÈRE C, MENETRIER M, PORTIER J, CAMPET G, DESHAYES A, FRISON J C, HWANG S J, SONG S W, CHOY J H. Relationship between chemical bonding nature and electrochemical property of $LiMn_2O_4$ spinel oxides with various particle sizes: “electrochemical grafting” concept [J]. The Journal of Physical Chemistry B, 1999, 103: 2100−2106.

[32] LI Li, BIAN Yi-fan, ZHANG Xiao-xiao, GUAN Yi-biao, FAN Er-sha, WU Feng, CHEN Ren-jie. Process for recycling mixed-cathode materials from spent lithium-ion batteries and kinetics of leaching [J]. Waste Management, 2018, 71: 362−371.

[33] HAN Chao, LI Wei-jie, WANG Jia-zhao, HUANG Zhen-guo. Boron leaching: Creating vacancy-rich Ni for enhanced hydrogen evolution [J]. Nano Research, 2022, 15: 1868−1873.

[34] YANG Sheng-hai, LI Hao, SUN Yan-wei, CHEN Yong-ming, TANG Chao-bo, HE Jing. Leaching kinetics of zinc silicate in ammonium chloride solution [J]. Transactions of Nonferrous Metals Society of China, 2016, 26(6): 1688−1695.

[35] WANG Chang-hong, JIANG Kai-qi, TIMOTHY W J, YANG Sheng-hai, YU Hai, PAUL F, LI Kang-kang. Electrowinning-coupled CO_2 capture with energy-efficient absorbent regeneration: Towards practical application [J]. Chemical Engineering Journal, 2022, 427: 131981.

[36] DEMIRKIRAN N, KÜNKÜL A. Dissolution kinetics of ulexite in perchloric acid solutions [J]. International Journal of Mineral Processing, 2007, 83: 76−80.

废三元锂离子电池正极材料脱锂渣的淀粉还原浸出动力学

李为轮[1]，陈永明[1]，李 帅[1]，王长红[1]，李 云[1]，赵天瑜[1,2]，
Michael TRAVERSY[2]，常 聪[1]，介亚菲[1]，何 静[1]，唐朝波[1]，杨声海[1]

1. 中南大学 冶金与环境学院，长沙 410083；
2. The Robert M. Buchan Department of Mining, Queen's University, 25 Union Street, Kingston, Ontario K7L3N6, Canada

摘 要：以淀粉为还原剂从废三元锂离子电池(LIBs)正极材料脱锂渣中回收 Ni、Co 和 Mn，并研究其浸出动力学和机理。系统地研究搅拌速率、浸出温度、H_2SO_4 浓度和淀粉用量对 Ni、Co 和 Mn 浸出率的影响。结果表明，在搅拌速率为 500 r/min、硫酸浓度为 1.5 mol/L、淀粉用量为 6 g/L、浸出温度为 80 ℃和浸出时间为 60 min 的优化条件下，Ni、Co 和 Mn 的浸出率分别达到 98.07 %、96.52%和 98.06%。根据冶金过程液固反应动力学模型，脱锂渣的浸出动力学可以用化学反应控制的未反应收缩核模型很好地进行描述。在浸出反应中，Ni、Co 和 Mn 的表观反应活化能分别为 93.32、102.84 和 95.68 kJ/mol，H_2SO_4 的表观反应级数分别为 0.9225、1.0335 和 1.1285。淀粉容易制取、成本低，可取代传统还原剂用于从废三元锂电池中提取有价金属。

关键词：废旧锂离子电池；浸出动力学；脱锂渣；H_2SO_4−淀粉溶液；化学反应控制

(Edited by Wei-ping CHEN)